SLAC – PUB – 3421
August 1984
(T/E)

# RECENT PARTICLE SEARCHES AT PEP*

R. L. MESSNER

*Stanford Linear Accelerator Center*
*Stanford University, Stanford, California, 94305*

Invited talk presented at the 6th International Conference on
High Energy Physics at Vanderbilt, Nashville, Tennessee, April 5–7, 1984

* Work supported by the Department of Energy, contract DE–AC03–76SF00515.

## 1. Introduction

The subject of this talk will be the recent searches for new particles that have been conducted at PEP. In such a context, PEP's unique advantage is a large integrated luminosity that has been accumulated in recent years. While the center of mass energy has remained at 29 GeV, experiments can perform clean, high statistics searches to set improved limits on new particle production.

## 2. TPC-Search for Charge $\frac{2}{3}$e and $\frac{1}{3}$e Particles

The orthodoxy of QCD provides no clear guidelines as to how free quarks might be produced; intuitive estimates [1] suggest that the cross section should be highly suppressed relative to typical hadron production, perhaps even favoring the production of diquark (uu) pairs. The TPC group has recently published results of its search for charge $\frac{4}{3}$e diquarks. [2] The search presented here for charge $\frac{1}{3}$e and $\frac{2}{3}$e particles is quite similar in spirit, except that an extended search region and increased statistics are available.

The time projection chamber (TPC) at PEP [3] identifies particle species by simultaneous measurement of a particle's ionization loss and its momentum with good resolution. The measured value of energy loss due to ionization, <dE/dx>, is defined to be the mean of the lowest 65% of the measured pulse heights, and scales as the square of the charges of the particle involved. The apparent momentum is determined by the track curvature in the magnetic field of the TPC, and scales as the charge of the particle, Q.

From an integrated luminosity of 77 $pb^{-1}$, approximately 30K events of the type $ee \rightarrow \gamma^* \rightarrow$ hadrons were selected. The sample contained an estimated 8% background coming from cosmic rays, beam gas, $\tau\tau$, and two photon processes. A scatter plot of <dE/dx> vs. apparent momentum for a subset of tracks from the

data sample is shown in Fig. 1. Bands corresponding to the familiar Q=1 particles e, $\mu/\pi$, K, p are clearly seen. The search was performed in two regions of the scatter plot not populated by the stable Q=1 particles, one below minimum ionization for Q=1 tracks and one at high apparent momentum and <dE/dx>. The boundary at <dE/dx> = 40 KeV/cm avoided effects of electronic saturation; the boundary at <dE/dx> = 4 KeV/cm isolated the region where the detector efficiency was well understood. Candidate tracks selected from the two search regions were required to have at least 80 samples of ionization more than 1 cm from the edge of a TPC sector and separated from other sources of ionization by at least 3 cm. A cut was applied limiting momentum assignment errors estimated from residuals to the fit to be less than 0.1 p. These cuts assured that the candidate tracks were well measured. 96 tracks, all from the search region above minimum ionization for Q=1 particles, remained. Possible backgrounds in this region are nuclear secondaries originating from interactions in the detector material and unresolved pairs of nearby tracks. After requirements designed to remove these backgrounds were imposed, no candidate tracks remained.

In Fig. 1 are shown the ionization curves expected for $Q = \frac{1}{3}$ and $Q = \frac{2}{3}$ particles with masses of 3 and 10 GeV/$c^2$. To compute the sensitivity of the experiment, a model for the production of fractionally charged particles is required; here QCD provides no clear theoretical guidance. Efficiencies were calculated using a modified Lund [4] event generator for which fractionally charged particles were introduced into multihadron events. Two momenta distributions for the fractionally charged particles were used: $dN/dp \approx \frac{p^2}{E}$ and $dN/dp \approx \frac{p^2}{E} e^{-3.5E}$.

The first spectrum is preferred from kinematical arguments and the expectation that free quarks will be quite massive; the second is typical for light hadron production. Limits for

$$R_Q \equiv \frac{\sigma(e^+e^- \rightarrow Q\bar{Q}X)}{\sigma(e^+e^- \rightarrow \mu^+\mu^-)}$$

are shown in Fig. 2 as a function of the quark mass. Typically, $R_Q < 0.01$; we also

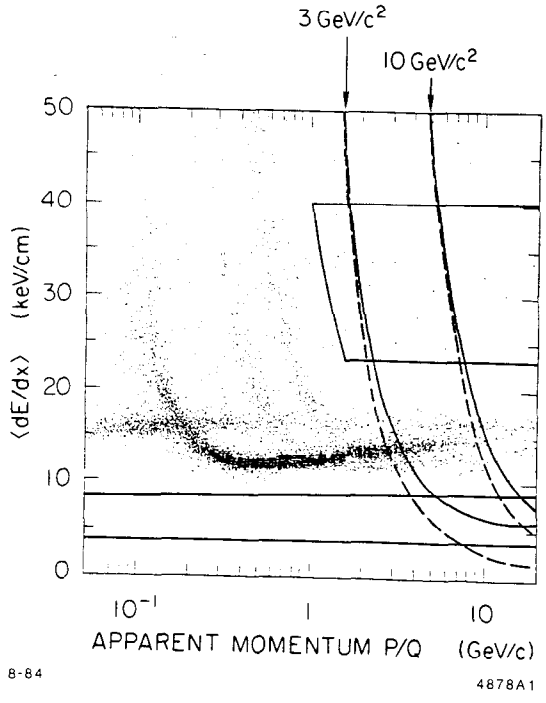


Fig. 1. Scatter plot of <dE/dx> vs. apparent momentum (p/Q) for tracks in the data sample. Two search regions are indicated. The lines are expected ionization curves for Q=2/3 (solid line) and Q=1/3 (dashed line) particles with masses of 3 and 10 GeV/$c^2$.

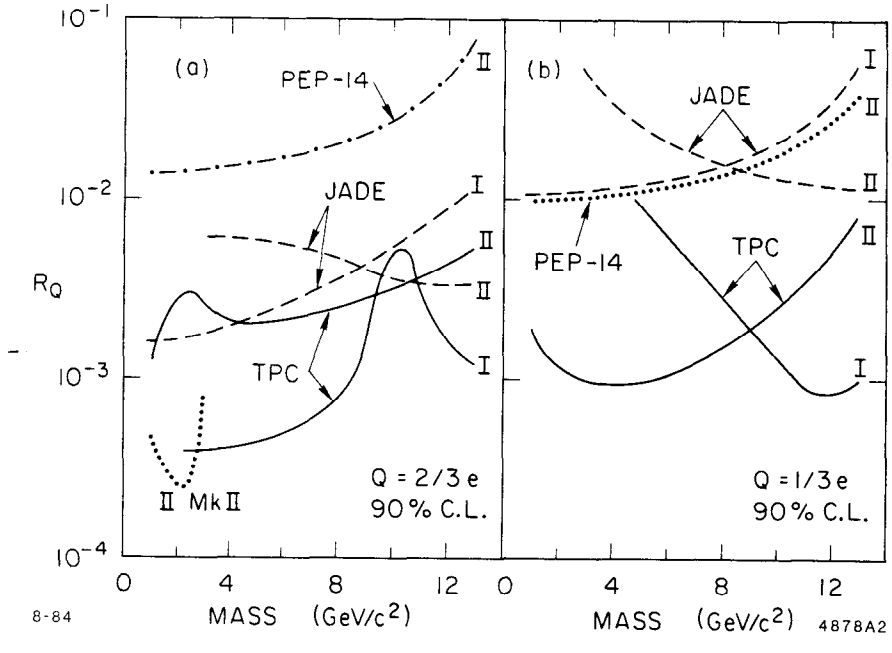


Fig. 2. Upper limit curves (90%C.L.) for $R_Q \equiv \frac{\sigma(e^+e^- \to Q\bar{Q}X)}{\sigma(e^+e^- \to \mu^+\mu^-)}$ for the production of Q=2/3 and Q=1/3 particles. Also plotted are the results of similar searches by the MARK II, Jade, and PEP-14 collaborations. The assumed momentum distributions are I: dN/dp $\sim p^2/E$ and II: dN/dp $\sim (p^2/E)e^{-3.5E}$.

point out that the published TPC result for $Q = \frac{4}{3}$ particles is also improved by a factor representing the increase in integrated luminosity, namely 3.5.

## 3. MAC - $e^+e^- \rightarrow \gamma\gamma$

The process $ee \rightarrow \gamma\gamma$ is unique among two body QED final states in that it is not modified to lowest order by contributions from weak interactions. A deviation from lowest order QED would involve new physics input. Previous studies [5] of $ee \rightarrow \gamma\gamma$ have looked for modifications to the QED cross section, which, for example, could be brought about by a new heavy electron that couples to $e\gamma$. It is customary to fit the data to a modified cross section given by two forms:

$$\frac{d\sigma}{d\Omega} = \frac{d\sigma_{QED}}{d\Omega}(1 \pm \frac{s^2 sin^2\theta}{2\Lambda_\pm^4})$$

and

$$\frac{d\sigma}{d\Omega} = \frac{d\sigma_{QED}}{d\Omega}\left(1 \pm \frac{s^2 sin^2\theta}{2\Lambda_\pm^4(1 + cos^2\theta)}\right)$$

In the first case, $\Lambda_+$ can be interpreted as a limit on the contribution of a heavy electron with mass $m_{E^*}$ and charge $e^*$; $\Lambda_+$ is given by $\Lambda_+ = m_{E^*}\sqrt{\frac{e}{e^*}}$. $\Lambda_-$, however, has no interpretation. The second case corresponds to a modification to the electron propagator, indicating a non-pointlike coupling between the electron and photon. This would require the electron to have substructure.

The possible observation of an abnormally large rate of $Z^\circ$ decay into a lepton pair and a hard photon [6] has led to speculation about the existence of a new spin 0 boson with mass $m_x \sim 50$ GeV produced in the reaction

$$Z^\circ \rightarrow X\gamma,\ X \rightarrow l^+l^-$$

If the X boson exists, it is expected to have a tensor coupling to photon pairs [7] which

would modify the differential cross section for $e^+e^- \rightarrow \gamma\gamma$ by adding an isotropic term,

$$\frac{d\sigma}{d\Omega} = \frac{d\sigma_{QED}}{d\Omega} + K_x$$

The constant term $K_x$ is proportional to the partial rates $\Gamma(X \rightarrow \gamma\gamma)$ and $\Gamma(X \rightarrow e^+e^-)$ and a function of s and $m_x^2$ of the Breit-Wigner form.

In order to extract the $e^+e^- \rightarrow \gamma\gamma$ signal, the MAC analysis requires:

1. No charged tracks in the Central Drift chamber.

2. Two energy clusters in the calorimeter with at least 70% of the energy contained in the electromagnetic section and a noncollinearity angle less than 10°.

3. The thrust axis of the event to have a polar angle $\theta$ greater than 30°.

In a sample corresponding to an integrated luminosity of $\sim$ 130 pb$^{-1}$, 23K events satisfied these requirements. The overall efficiency for extracting the events has been estimated to be $\sim$ 95%, essentially independent of angle. Background events from cosmic ray interactions as well as other final states of $e^+e^-$ annihilation were estimated to be less than 1% with visual scanning and Monte Carlo simulation. Radiative corrections up to order $\alpha^3$ were calculated using the Berends and Kleiss computer codes and applied to the data.

Figure 3 shows the corrected angular distribution for the $\gamma\gamma$ sample; the error bars represent the statistical errors added in quadrature with the estimated point-to-point systematic errors ($\sim$ 2%). In addition, there is an overall systematic normalization error comprised of $\pm$ 1.5% due to uncertainties in the corrections and $\pm$ 3.6% in the luminosity measurement. The bottom of the figure shows the ratio of the measured distribution to the prediction of QED, along with theoretical curves corresponding to $K_x = 0$, 1.5 and 3 pb/sr. The result is in good agreement with QED, and we extract the limit $K_x < 1.56$ pb/sr at the 95% confidence level, which is model independent.

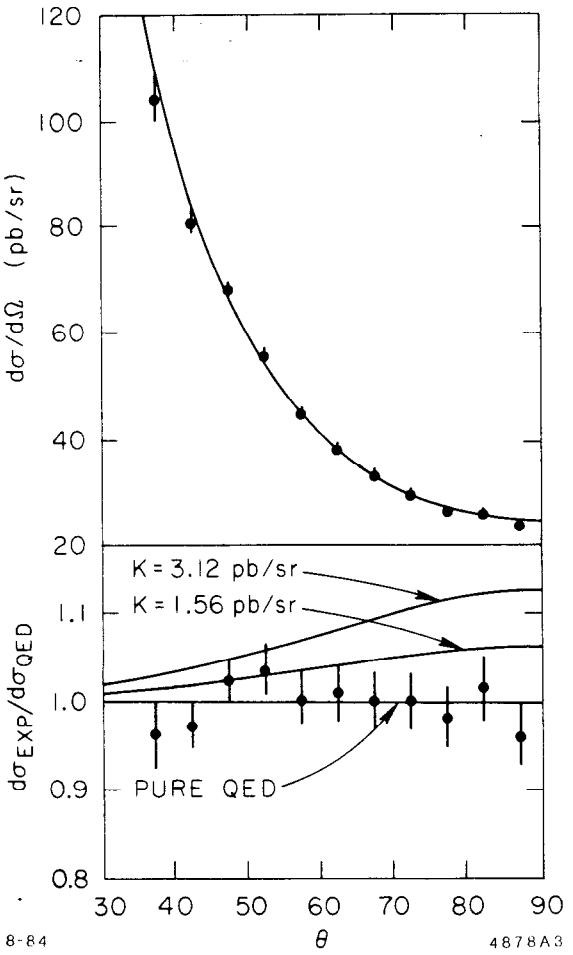


Fig. 3. MAC $e^+e^- \rightarrow \gamma\gamma$ data together with the QED prediction. Below the data is divided by the QED prediction; curves showing limits on contributions from a term constant in $\theta$ are indicated.

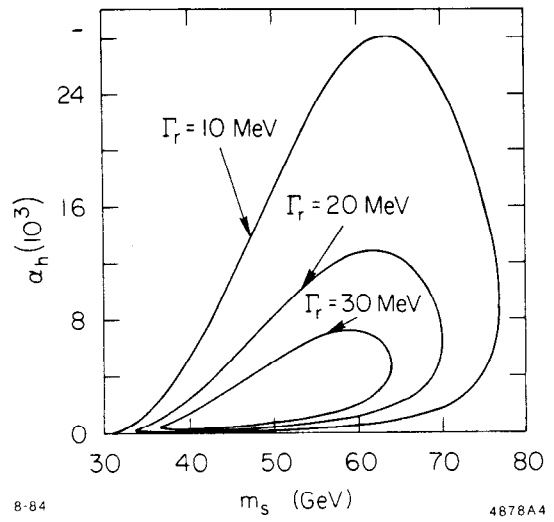


Fig. 4. Allowed regions in the $\alpha_H$ vs. $m_x$ plane for various values of $\Gamma_r \equiv \Gamma(Z^\circ \rightarrow e^+e^-\gamma)$.

Fits for $\Lambda$ were performed using the modified cross sections. The modifications affect the overall normalization as well as the shape of the distribution; the $\chi^2$ function for the fit treated separately the point-to-point errors and the normalization errors. The results are summarized below for the 95% confidence level limits on $\Lambda$ :

| | Excited Electron (GeV) | Modified Propagator (GeV) |
|---|---|---|
| $\Lambda_+$ | 66 | 62 |
| $\Lambda_-$ | 67 | 64 |

These are a substantial improvement over previous PEP limits.[5] In view of the fact that $ee \to \gamma\gamma$ is used to provide absolute normalization for processes which do have modifications from weak interactions, [8] it is worthwhile to update the tests of the QED prediction.

One may use constraints from the measured width for $Z^\circ \to e^+e^-\gamma$ ($\Gamma_r$) together with the limit for $K_x$ given above to determine allowed regions in the $\alpha_h = 2\Gamma(X \to e^+e^-)\ m_x$ vs. $m_x$ plane, as shown in Fig. 4. The contours assume $K_x =$ 1.5 pb/sr. For the preferred value of $m_x$, on the order of 45 GeV, the contours are a factor of 10 larger in $\alpha_h$ than those determined by similar analyses at PETRA. This is due to rapid decline in sensitivity at lower beam energies. The interested reader is refered to the summary of PETRA results presented at this conference. [9]

## 4. Supersymmetry Searches

Supersymmetric theories postulate a basic symmetry between bosons and fermions in nature. For every familiar particle of the standard model there should be supersymmetric partners with spin differing by $\frac{1}{2}$ unit and, in the case of exact

supersymmetry, identical mass. [10] Since none of these particles has yet been found, the symmetry, if valid, is badly broken. The details of how this breaking occurs are model dependent, and there is no universal agreement as to the mass spectrum of supersymmetric particles. [11] Depending upon the particular model, masses and lifetimes of the particles can vary, requiring a variety of experimental techniques for their production and detection.

Until this past year, SUSY searches have been limited to pair production processes for which the SUSY particle mass must be less than the beam energy for it to be produced. The reported null results indicate that the masses of SUSY particles must be greater than 20 GeV.[9] The MAC and MARK II collaborations have searched for processes which extend the experimental sensitivity to mass ranges greater than the beam energy. One process, $e^+e^- \rightarrow \gamma\tilde{\gamma}\tilde{\gamma}$ has the potential to probe selectron masses up to 50 GeV/$c^2$.

The first reaction we will talk about [12] is $e^+e^- \rightarrow e^{\pm}\tilde{e}^{\mp}\tilde{\gamma}$ followed by the decay $\tilde{e}^{\mp} \rightarrow e^{\mp}\tilde{\gamma}$; the Feynman graphs are shown in Fig. 5. One assumes that the photino is stable and does not interact in the detector; the selectron is produced practically at rest in the center of mass frame, and consequently the electron from its decay will have high energy ($\sim \frac{m_{\tilde{e}}}{2}$) and an almost flat angular distribution. Since the beam-related $e^{\pm}$ in the final state will be scattered preferentially at a very small angle, it escapes undetected down the beam pipe. The signal, then, for the detection of a selectron by this reaction is an isolated high energy electron, typically with large transverse momentum, observed in the detector.

The experimental concern is to assure that the observed electron is truly isolated. QED processes, for example, $ee \rightarrow ee\gamma$ or $ee \rightarrow \tau\tau$, are copious sources of high energy electrons unless efficiently vetoed. The method to solve this situation is to define a kinematic search region for which ordinary electron sources will of necessity have been tagged. The definition of the search region consequently will depend upon

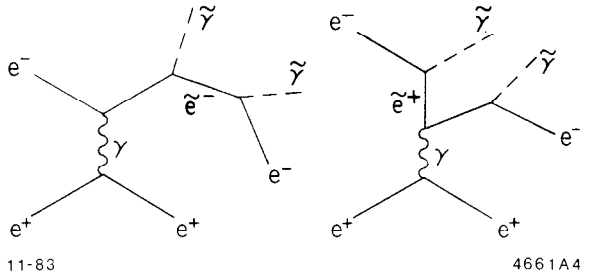


Fig. 5. Diagrams for production of a single selectron in $e^+e^-$ annihilation.

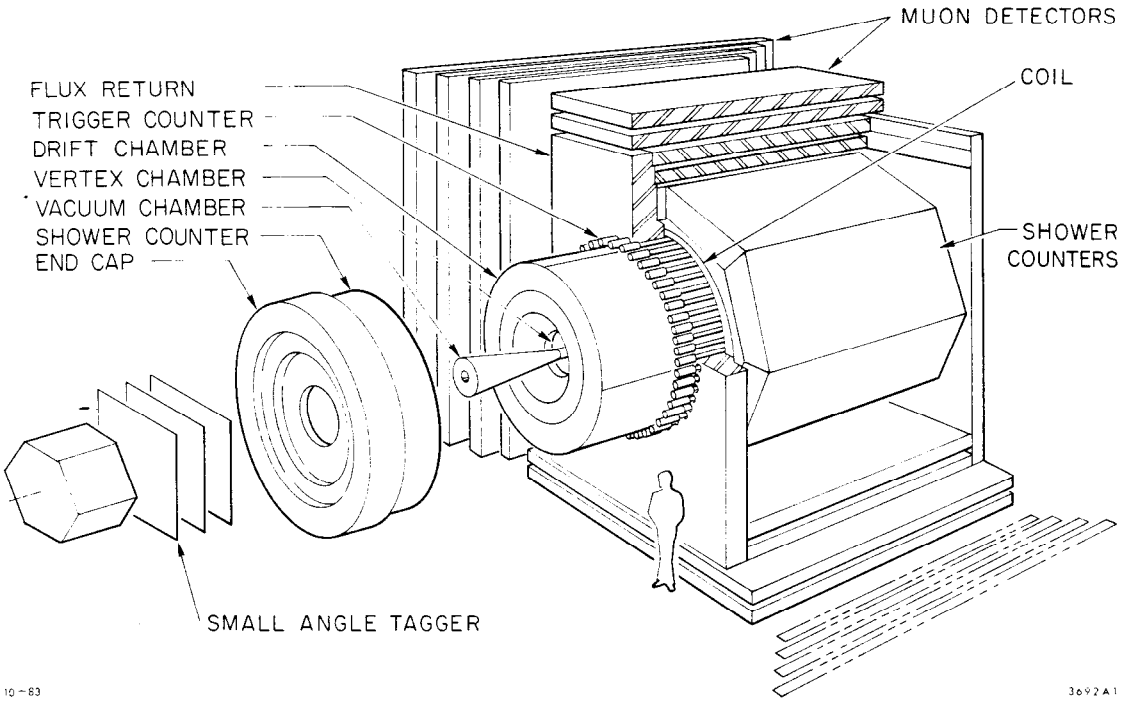


Fig. 6. Isometric view of the MARK II detector.

a particular experiment's veto capabilities.

## 4.1 MARK II - SINGLE $\tilde{e}$ PRODUCTION

The features of the MARK II detector have been described in detail; [13] [14] a view of the detector is given in Fig. 6. The essential features consist of a high precision vertex drift chamber and a main drift chamber which detect charged particles to within 10° of the beam axis, and electromagnetic calorimetry which is divided into three subsystems: a small angle tagging system, endcap calorimeters, and a central liquid argon calorimeter. The liquid argon (LA) system consists of eight modules surrounding the magnet coil and has an angular acceptance of $|\cos\theta| < 0.70$ relative to the beam axis. The endcaps cover the region $0.75 < |\cos\theta| < 0.92$, but have a substantial break in their azimuthal coverage due to their support stands. The small angle tagging system covers the region between 2° and 4° from the beam axis.

The trigger for electron candidates required a single track which deposited at least 1 GeV in a single LA module. Further analysis of the events obtained by the trigger required that the track fall within the active area of the LA module and to deposit at least 6 GeV. Cosmic ray showers were eliminated by a cut on the number of drift chamber hits and a requirement that the prong originate from the beam interaction point. Events with extra low angle particles were eliminated by the use of the vertex chamber information and a requirement that the small angle tagging system have less than 3 GeV in any module.

At this stage, the major sources of background are QED processes, particularly $ee\gamma$ events for which one electron is detected, one electron goes down the beam pipe, and the gamma falls into an insensitive region of the detector. The $ee\gamma$ hypothesis for single prong events may be tested if one utilizes the three body character of the hypothesis to determine the gamma direction by including the information that the unseen electron had to be within 2° of the beam axis. Moreover, the single prong

event analysis can be calibrated by the use of ee$\gamma$ events for which the single gamma had been detected, i.e., had not fallen into insensitive regions of the detector.

The study of the calibration sample showed that ee$\gamma$ feedthrough could be eliminated by requiring that the recoil angle for the hypothetical gamma derived from a three body hypothesis be located well within the LA calorimeter. The effect of all cuts used in the analysis is to constrain the single prong events to lie within the contour shown in Fig. 7; the efficiency for high mass selectrons was calculated to be $\sim$ 40%. Additional backgrounds from processes such as ee$\gamma\gamma$, $\tau$ production, and two photon processes were found to be small.

The search region shown in Fig. 7 yielded no final candidates for an integrated luminosity of 123 pb$^{-1}$ for a 95% confidence level upper limit on the cross section within the acceptance of $2.4 \times 10^{-2}$ pb. Using the production cross section of Ref. 12 the upper limit on the cross section gives a lower limit on the mass of the selectron of

$$m_{\tilde{e}} > 22.2 \ GeV/c^2,$$

where the right-handed and left-handed selectrons are assumed to be degenerate. If one partner is infinitely heavy, the cross section for producing a selectron is effectively halved, and the mass limit for the lighter selectron becomes 19.4 GeV/c$^2$.

### 4.2 MAC - Single $\tilde{e}$ Production

The configuration of the MAC detector is particularly well suited for the detection of processes involving missing energy and momentum. A diagram of the apparatus is shown in Fig. 8. The central portion of the detector consists of a central drift chamber (CD) surrounded by a hexagonal barrel of shower counters and hadron calorimeters. The endcap portion of the detector contains scintillation counters and calorimeter modules which provide efficient coverage to within 9° to 12° of the beam

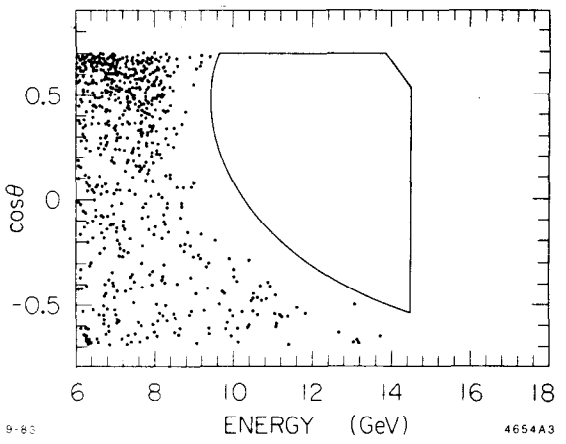


Fig. 7. MARK II acceptance for single negative prongs. Also shown is a scatter plot of single-prong events.

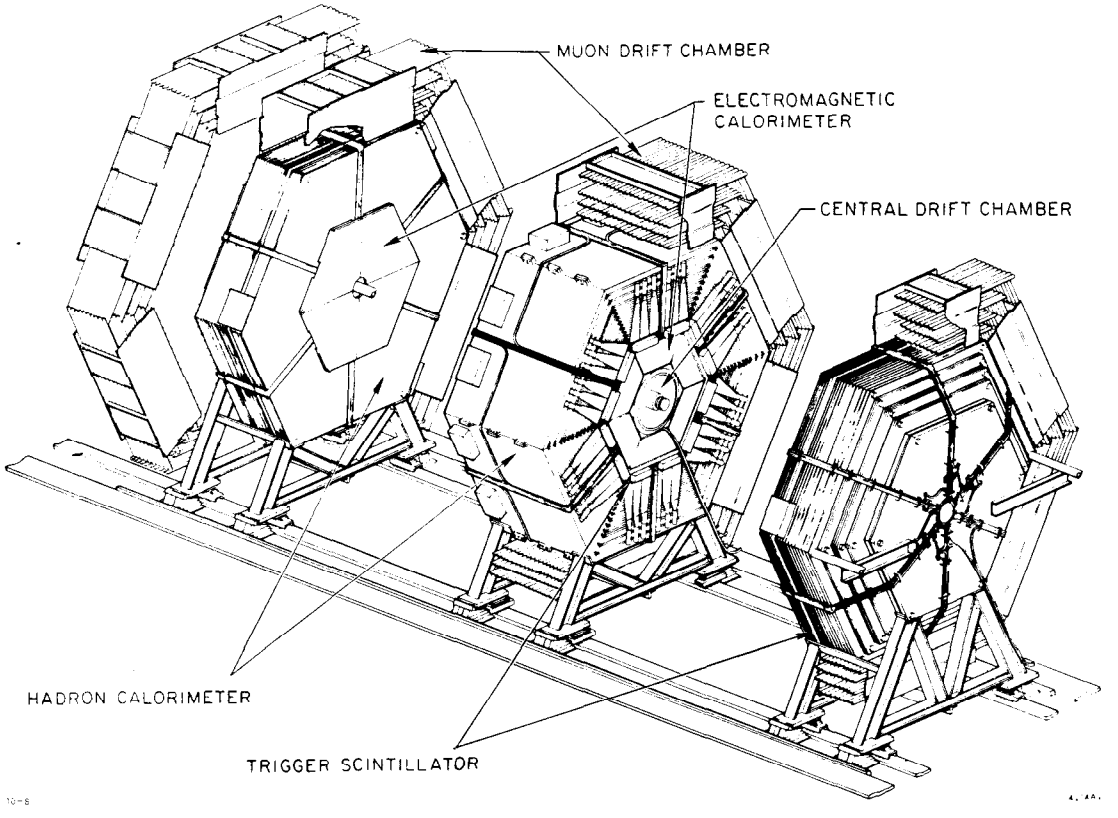


Fig. 8. Isometric view of the MAC detector.

direction. During the summer of 1983 a veto calorimeter package was installed to extend the coverage to within 5° of the beam axis.

Unobserved particles from QED processes are restricted to small angles around the beam axis. Momentum conservation consequently confines the energy and angle of an isolated electron observed in the detector which originates from QED sources. The data reported here consist of two sub-samples corresponding to data taken before (36 $pb^{-1}$) and after (30 $pb^{-1}$) the installation of the veto calorimeter package. The analysis required a single prong with momentum $> 1$ GeV/c and $|\cos\theta| < 0.75$ to be associated with shower energy $> 3$ GeV (2 GeV for the second data sample). Events with more than one CD track, an additional shower in the central or endcap calorimeters, or an endcap scintillator hit were removed. The efficiency of the trigger, which required only a minimum energy deposition in the central shower counter, was measured from the real data sample, with use of $ee \rightarrow ee\gamma$ events that have only one particle in the central section and satisfy other MAC triggers. The overall efficiency for single electron events was calculated to be 92% at 3 GeV and 95% at or above 6 GeV.

As shown in the insert to Fig. 9, electrons produced by the $\tilde{e}$ decay tend to have energies $> 7$ GeV. The energy distribution of the single electron data from the first sample is also shown; the shape is consistent with the expected distribution from ee$\gamma$ events, and there are no events with an electron energy of more than 6 GeV.

The veto calorimeter package covered the angular range between 5° and 17° of the beam direction. The energy deposited in the calorimeter in association with single electron events from the second data sample are shown in Fig. 10. Single electron events with veto calorimeter energy greater than 0.25 GeV were rejected as ee$\gamma$ background. Studies of beam related occupancy of the veto calorimeter indicate that $< 1.4\%$ of true $\tilde{e}$ events would be rejected by this cut. For comparison, the electron energy distribution for the two single electron data samples are shown in Fig. 11. The

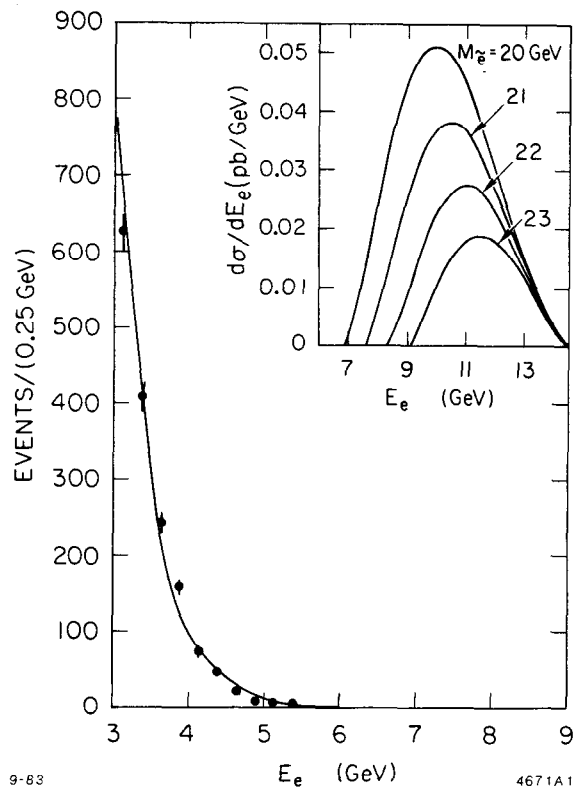


Fig. 9. MAC energy distribution of single electron events for a data sample of 36 $pb^{-1}$. A calculation of $ee \rightarrow ee\gamma$ is shown as the solid curve. The insert shows the expected energy distribution of single electrons from $\tilde{e}$ decay.

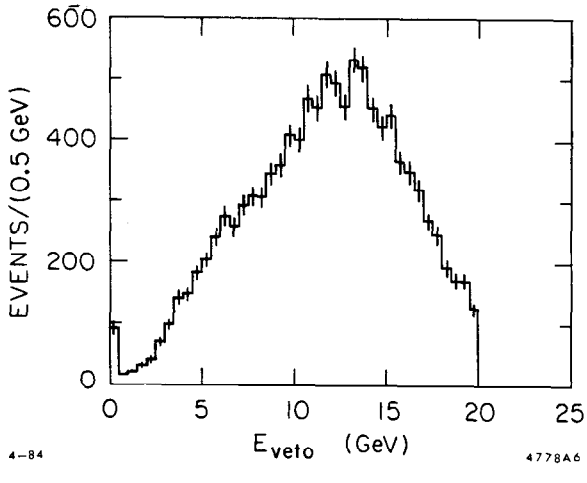


Fig. 10. Energy distribution in the veto calorimeters for single electron candidates. Events with $E_{veto} >$ 0.25 GeV were rejected as $ee\gamma$ background.

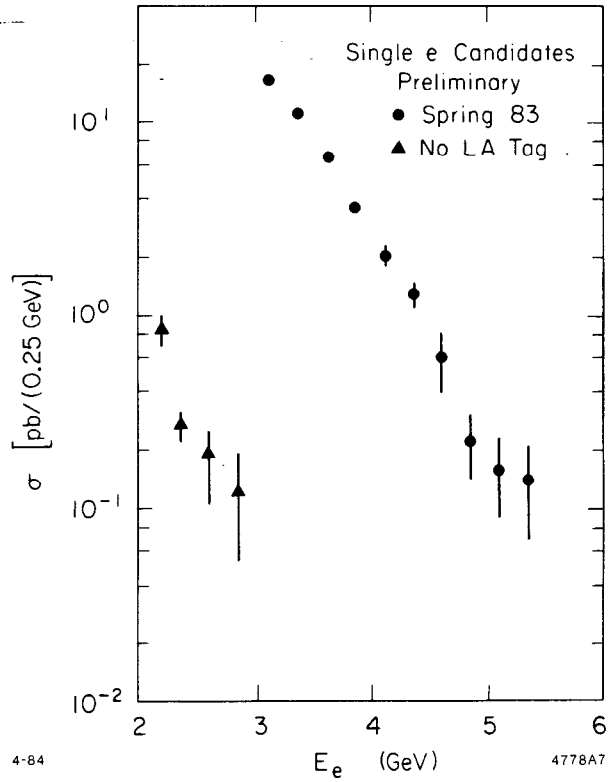


Fig. 11. Energy distribution of single electrons in the MAC detector. In the first data sample extra electrons and photons could be detected to within 9°–12° of the beam (dots). In the second sample, electrons and photons could be detected to within 5° of the beam (triangles).

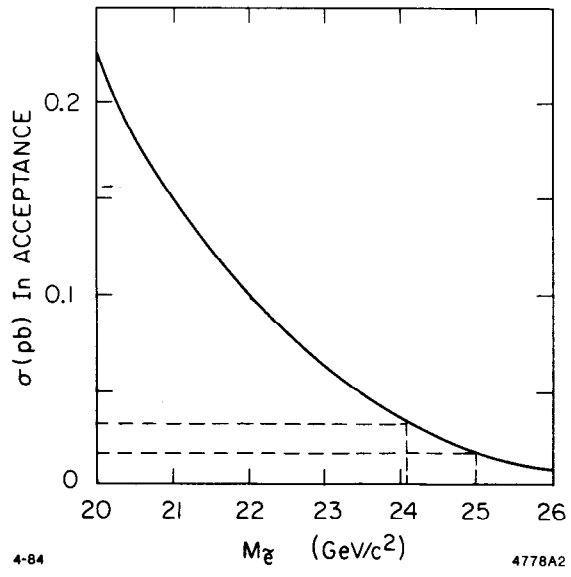


Fig. 12. Cross section in the MAC acceptance of single electons from $\tilde{e}$ decays as a function of the $\tilde{e}$ mass. The MAC upper limit corresponds to $m_{\tilde{e}} > 23.4$ GeV/$c^2$.

veto calorimeter suppresses ee$\gamma$ background so that the maximum electron energy observed is $< 3$ GeV.

Combining the two data samples, the upper limit on the single electron cross section in the MAC search region was $4.8\times10^{-2}$ pb at the 95% confidence level. The corresponding mass limit is $m_{\tilde{e}} > 23.4$ GeV/$c^2$, where the right-handed and left-handed selectrons are assumed to be degenerate. If one partner is infinitely heavy, the mass limit for the lighter selectron becomes 22.1 GeV/$c^2$. Increases to the total integrated luminosity will not significantly improve the $\tilde{e}$ mass limit, as can be seen in Fig. 12, which shows the $\tilde{e}$ cross section for the MAC acceptance as a function of the $\tilde{e}$ mass at current PEP energies. A doubling of the luminosity would extend the mass limit by only 5%. Further improvements on the $\tilde{e}$ mass limit have to come from different reactions or higher energies. The JADE group has reported a preliminary limit of 25 GeV/$c^2$ using the single electron technique.[9]

### 4.3 Photino Production

The second reaction being investigated by the MAC Collaboration is $e^+e^- \rightarrow \tilde{\gamma}\tilde{\gamma}\gamma$. [15] This process is simply the radiative correction to $e^+e^-$ annihilation into photino pairs, with the photon serving as the tag for the event, since the photinos are assumed to be stable and not to interact in the detector. In practice, the final state can be a photon with any set of neutral penetrating particles which are invisible to the detector. In particular, the neutrino counting reaction $ee \rightarrow \nu\bar{\nu}\gamma$ [16] is indistinguishable from photino production and limits the selectron mass regions that may be probed.[10] An anomolous rate for isolated single photon production would be a discovery whose precise nature would have to be investigated in further experiments.

The cross section for radiative photino production is sensitive to the selectron mass because it appears in the propagator as indicated in Fig. 13, and is also sensitive to the photino mass, which typically is assumed to be small. Recently, several calcu-

lations have been reported giving the cross section for arbitrary $\tilde{e}$ and $\tilde{\gamma}$ masses. [17] The results from one calculation are shown in Fig. 14, which gives the cross section assuming $m_{\tilde{\gamma}} = 1$ GeV/c$^2$ for a selection of $\tilde{e}$ masses as a function of $\sqrt{s}$. Also shown is the cross section for ee$\rightarrow \nu\bar{\nu}\gamma$ assuming $N_\nu$, the number of light neutrino species, is 3. Comparing the curves, it is clear that the ratio of radiative photino production signal to $\nu\bar{\nu}\gamma$ "background" is better at lower energies. This reaction is ideally suited for study at PEP.

Following the discussion of single electron production, QED processes, particularly $ee\gamma$, are potential sources of background for $ee \rightarrow \tilde{\gamma}\tilde{\gamma}\gamma$. Since the photon is Bremsstrahlung in origin, it does not peak at a definite energy, but instead has a broad 1/k spectrum. The veto detectors are employed to limit the angle of the leptons and consequently the transverse energy spectrum of the background and allows a search region to be defined. The method applies to other QED processes as well, e.g., $ee \rightarrow \gamma\gamma\gamma$, $ee \rightarrow \tau\tau\gamma$, etc. Finally, it should be pointed out that the single electron analysis can be used as a calibration of the veto system's performance for rejecting QED background. High transverse energy electrons and photons from $ee\gamma$ have very similar spectra, with the electrons being produced at a rate roughly ten that of the photons.

Other possible sources of background include cosmic rays and proportional chamber noise which can mimic photon showers. The central portion of the MAC detector is effectively encapsulated in an active shield of muon drift tubes and hadron calorimetry. Noise in the system produces an energy profile which does not follow the characteristic development of electromagnetic showers. Fig. 15 shows the hadronic energy of single photon and single electron candidates, the latter being used as a measure of the efficiency of the cuts. The requirement that less than 2 GeV of hadronic energy accompany the shower eliminated most of the cosmic rays while rejecting only 2% of the real photons. Additional cuts required that the photon candidates point

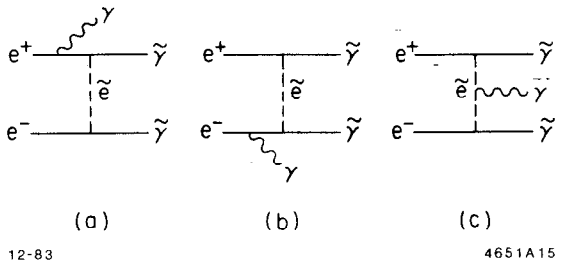


Fig. 13. Graphs for $e^+e^- \to \tilde{\gamma}\tilde{\gamma}\gamma$.

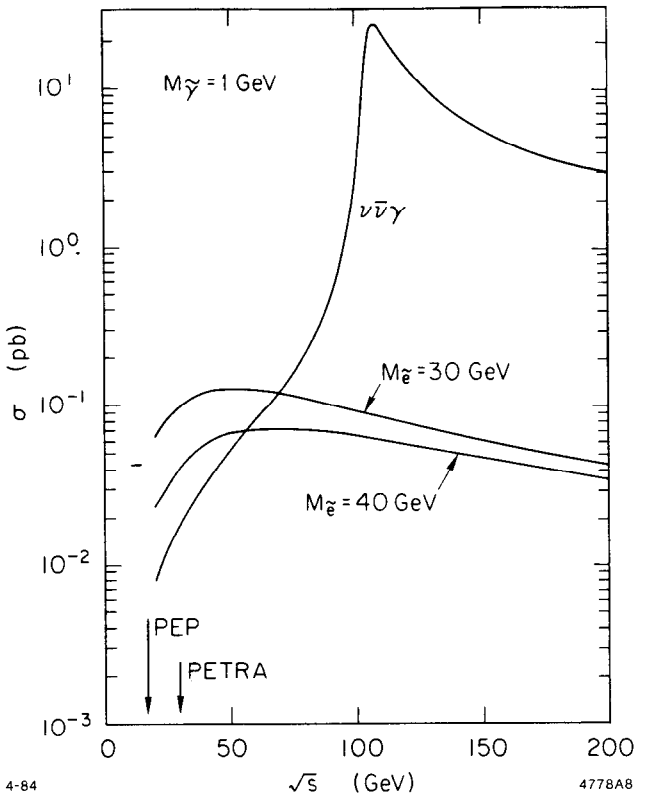


Fig. 14. Cross sections for single $\gamma$ events from the reactions $ee \to \tilde{\gamma}\tilde{\gamma}\gamma$ and $ee \to \nu\bar{\nu}\gamma$ assuming $N_\nu = 3$, $m_{\tilde{\gamma}} = 1\ \mathrm{GeV/c^2}$, $E_\gamma > 0.2\ E_{beam}$, and $|cos\theta_\gamma| < 0.94$.

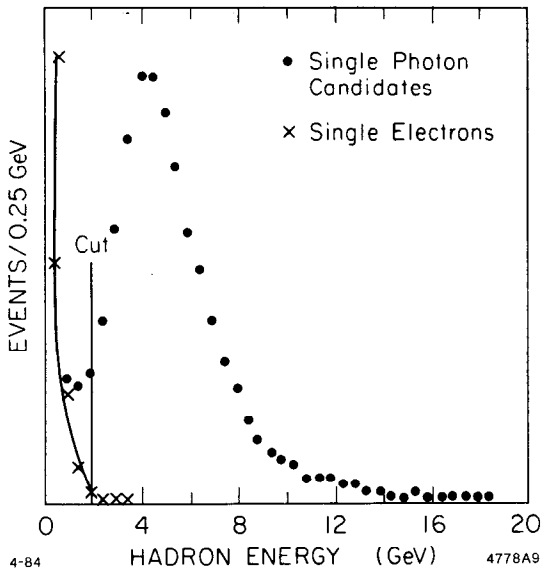


Fig. 15. Hadronic energy of single electron and photon candidates. A cut of 2 GeV eliminates most of the cosmic ray backgrounds.

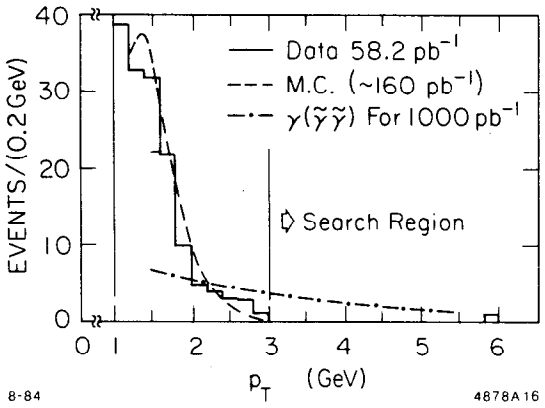


Fig. 16. $p_T$ distributions of single photon candidates. The expected background from $ee\gamma$ is shown as solid curves; the data had a veto angle of 5°. For reference the distribution from $ee \rightarrow \tilde{\gamma}\tilde{\gamma}\gamma$ is shown.

back to the beam crossing region and to have a transverse profile compatible with electron showers.

Again, the data presented comes from two subsamples with different veto coverages. For the data collected with the veto calorimeter package, typically $10^6$ triggers would be reduced to a sample of 400 events which could be scanned by physicists. Of these, 140 single photon events remained, the rest being cosmic rays, multi-gammas, chamber noise, or beam splash. The analysis required one photon shower with $40° < \theta < 140°$ and $\phi > 3°$ from a shower chamber boundary. No reconstructed central drift tracks were allowed. The overall efficiency of the analysis is estimated to be $\sim 60\%$. Fig. 16 shows the transverse momentum distribution of the single photon sample for 58 $pb^{-1}$ of data collected with the veto calorimeter package installed in the detector. The search region is defined as $p_T > 3.0$ GeV/c (the earlier sample used $p_T > 4.3$ GeV/c). [18] The data agree well with Monte Carlo estimates of the QED distribution for data taken with a 5° veto, except for one isolated event with a $p_T$ of 5.8 GeV/c. A view of the event and its shower profile is given in Fig. 17. Examination of the detector components showed no evidence for significant activity except for an assortment of muon drift tube hits around the beam pipe at one end of the detector. However, attempts to reconstruct a track from the hits in the outer muon system have been unsuccessful. It is relevant to point out that the measured transverse momentum of the photon would imply that $ee\gamma$ sources of photon background would be rejected at levels of 1 in $10^6$ or better, and that there should be activity in the veto calorimeter package and the endcap system. No evidence for failure of either system was found. In addition, the uncorrelated nature of the muon system activity is consistent with noise originating from the PEP RF system, although the probability for this occuring in coincidence with an event is relatively low ($\sim 10\%$). Finally, the usual caveats that apply to single events are also relevant here.

At this stage in the analysis, MAC has treated the event as a background for

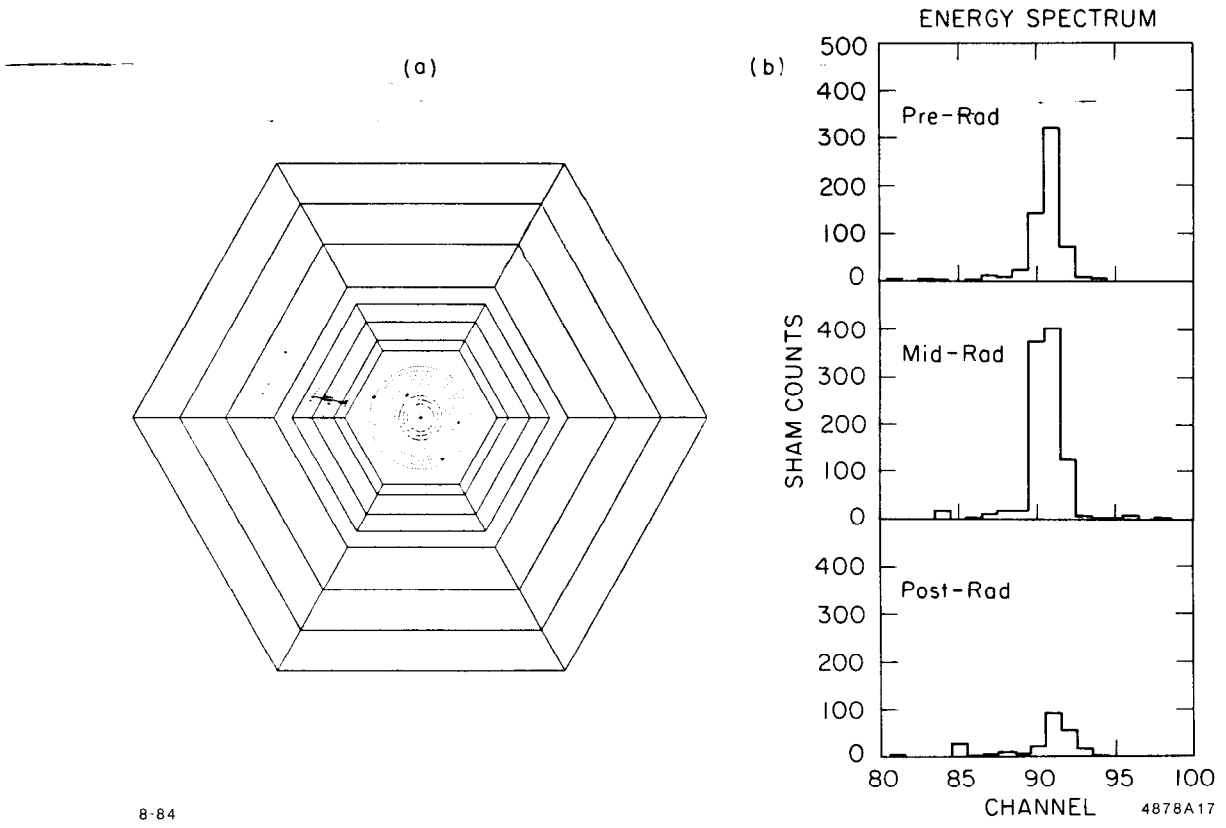


Fig. 17. Single photon event in the MAC detector. At right is the energy profile of the photon in the shower counter.

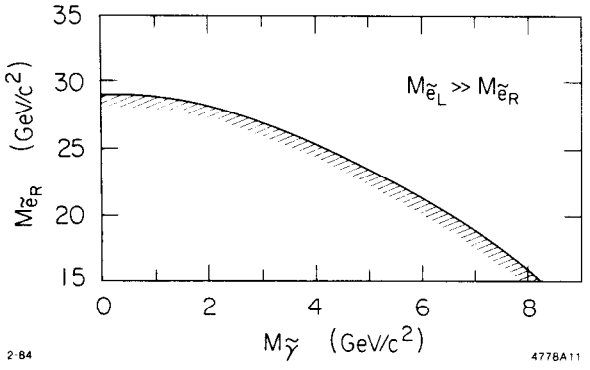


Fig. 18. Region in the $m_{\tilde{e}}$ vs. $m_{\tilde{\gamma}}$.

the purpose of quoting limits. It is important to note that the integrated luminosity is sufficiently large that the search is sensitive to certain backgrounds, particularly $\nu\bar{\nu}\gamma$. Calculations provide the following estimates or limits for contributions to the single photon search region:

$$ee \rightarrow \nu\bar{\nu}\gamma \sim 0.4 \text{ event}$$
$$ee \rightarrow \tau\tau\gamma \sim 0.03 \text{ event}$$
$$ee \rightarrow \mu\mu\gamma < 0.3 \text{ event}$$
$$ee \rightarrow ee\gamma < 0.2 \text{ event}$$

Assuming one background event the combined data set gives the following preliminary limits at the 90% confidence level:

$$N_\nu < 51$$

for the number of neutrino species; and

$$m_{\tilde{e}} > 28.5 \; GeV/c^2$$

if one partner is infinitely heavy, or

$$m_{\tilde{e}} > 33.7 \; GeV/c^2$$

if the right-handed and left-handed selectrons are degenerate. Note that the above limits assume that the $\tilde{\gamma}$ mass is massless. The excluded regions for the more general case of non-zero $\tilde{\gamma}$ mass can be seen in Fig. 18.

## 5. Acknowledgments

I would like to thank the members of the TPC, MARK II, and MAC collaborations for sharing their results. I have benefitted from discussions with Dave Ritson, Henry Band, Kwong Lau and Richard Prepost.

## References


1. A. DeRujula, R. Giles, and R. Jaffee, Phys. Rev. D17, 285 (1978); R. Slansky, T. Goldman, and G. Shaw, Phys. Rev. Lett. 47, 887 (1981).

2. H. Aihara, et al., Phys. Rev. Lett. 52, 168 (1984).

3. PEP-4 collaboration, IEEE Trans. Nucl. Sci. 30, 63, 76, 162 (1983); A. Barbara-Galtieri, SLAC-Report-250, 36 (1982); G. R. Lynch and N. J. Hadley, SLAC-Report-250, 85 (1982).

4. B. Andersson and G. Gustafson, Z. Phys. C3, 223 (1980).

5. S. Yamada, "Search for New Particles," in Proceedings of the 1983 International Symposium on Lepton and Photon Interactions at High Energies, Cornell University; K. Lau, SLAC-Report-259 (1983).

6. G. Arnison, et al., UA1 collaboration, CERN-EP-83-162; UA2 collaboration, P. Bagnaia, et al., Phys. Lett. 129*B*, 130 (1983).

7. W. Hollick, F. Schrempp, and B. Schrempp, DESY 84-011 (1984); F. W. Bopp, et al., SI 84-3 (1984).

8. MAC collaboration, "A High Precision Measurement of the $e^+e^- \rightarrow e^+e^-$ Angular Distribution at $\sqrt{s} = 29$ GeV," paper submitted to 22nd Inter. Conf. on HEP, Leipzig, 1984.

9. W. Krenz, Talk presented at this conference.

10. H. Haberand, G. L. Kane, UM-HE-TH 83-17; S. Rudaz, Talk presented at this conference.

11. P. Fayet in "Unification of the Fundamental Particle Interactions," eds. S. Ferrara, J. Ellis and P. Van Nieuwenhuizen (Plenum Press, N.Y., 1980), p.

587; L. E. Ibanez and G. G. Ross, Phys. Lett. 110*B*, 215 (1982); J. Ellis, L E. Ibanez and G. G. Ross, Phys. Lett. 113*B*, 283 (1982); J. Ellis, C. Kounnas, D. V. Nanopoulos, CERN-TH-3824 (1984).

12. M. K. Gaillard, L. Hall, and I. Hinchliffe, Phys. Lett. 116*B*, 279 (1982).

13. L. Gladney, et al., Phys. Rev. Lett. 51, 2253 (1983).

14. R. H. Schindler, et al., Phys. Rev. D24, 78 (1981).

15. J. Ellis and J. S. Hagelin, Phys. Lett. 122*B*, 303 (1983); K. Grassie and P. N. Pandita, DO-TH 83-24; J. Ware and M. E. Machacek, NUB-2626 (1984).

16. E. Ma and J. Okada, Phys. Rev. Lett. 41, 287 (1978) and Phys. Rev. D18, 4219 (1978); K. J. F. Gaemers, R. Gastman, and F. M. Renard, Phys. Rev. D19, 1605 (1979).

17. K. Grassie and P. N. Pandita, DO-TH 83-25; J. Ware and M. E. Machacek, NUB-2626 (1984).

18. H. R. Band, SLAC-PUB-3335 (1984); M. Piccolo, SLAC-Report-267, 673 (1983).